Arch. Mech., **66**, 4, pp. 269–286, Warszawa 2014

Effect of hydrogen injection into natural gas on the mechanical strength of natural gas pipelines during transportation

S. ELAOUD[1)], B. ABDULHAY[2)], E. HADJ-TAIEB[1)]

[1)] *Laboratory of Applied Fluids Mechanics*
Process and Environment Engineering, ENIS
P.O. Box, W, Sfax, 3038, Tunisia
e-mail: elaoudsa@yahoo.fr

[2)] *Lebanese International University*
School of Engineering
Energy and Thermo-Fluids Research Group
P.O. Box 146404, Mazraa, Beirut, Lebanon

The aim of this paper is to study the effect of hydrogen injection into natural gas transient flows on the mechanical strength of natural gas pipelines. The governing equations of hydrogen-natural gas mixtures are two nonlinear partial differential equations. The fluid pressure and velocity are considered as two principal dependent variables. The fluid is a homogeneous hydrogen-natural gas mixture for which the density is defined by an expression averaging the two gas densities where an adiabatic process is admitted for the two components. The problem has been solved by the nonlinear method of characteristics. By the use of Laplace's law, the pipe's circumferential stress has been analyzed for different hydrogen mass fraction in the mixture. It was then compared to the allowable stress of different grade pipeline steels used to transport natural gas. The obtained results have shown that the allowable stress for the natural gas pipelines is exceeded for some fractions of hydrogen in the hydrogen-natural gas mixtures.

Key words: hydrogen-natural gas mixtures, transient flow, method of characteristics, circumferential stress.

Notations

C celerity of waves ($\mathrm{m}\cdot\mathrm{s}^{-1}$),
C_p specific heat at constant pressure for hydrogen or for natural gas ($\mathrm{J}/(\mathrm{Kg}\cdot{}^\circ\mathrm{K})$),
C_V specific heat at constant volume for hydrogen or for natural gas ($\mathrm{J}/(\mathrm{Kg}\cdot{}^\circ\mathrm{K})$),
D pipeline diameter (m),
e thickness of the pipe (m),
L pipe length (m),
p pressure (bar),
t time (s),
V celerity (m/s),

x space coordinate (m),
Δx space interval (m),
γ' $\gamma' = C_p/C_V$, specific heats ratio for natural gas,
γ $\gamma = C_p/C_V$, specific heats ratio for hydrogen,
λ friction factor,
θ hydrogen mass fraction (dimensionless),
ρ density (Kg/m^3),
σ allowable strength (MPa),
σ_u ultimate strength (MPa),
σ_y yield strength (MPa).

Subscripts
0 steady state,
g natural gas,
h hydrogen.

1. Introduction

Hydrogen will play a decisive role in many future energy systems. The possible use of existing natural gas pipeline networks for mixtures of natural gas and hydrogen offers a unique and cost-effective opportunity to initiate the progressive introduction of hydrogen as a part of the development of a full hydrogen energy system. As the thermodynamic properties of hydrogen differ significantly from those of natural gas, it is not at all possible to simply use the existing pipelines to pump hydrogen and hydrogen-natural gas mixtures. For these reasons, many researches have been performed to see the effect of hydrogen on natural gas network. In particular, one can cite the works which have clarified the hydrogen permeation mechanism through a steel pipe's wall [1] and the works which study the influence of gaseous hydrogen under internal pressure in notched pipes [2]. In addition to these studies, the effect of hydrogen injection into natural gas on the mechanical strength of the existing pipelines and on the pressure evolution, during transportation, should be correctly predicted. In fact, the work presented in [3] has shown that the transient pressure oscillations for hydrogen and hydrogen-natural gas mixtures are higher compared to those for natural gas. However in this study, the celerity of waves has been determined based on the assumption of a rigid model. In this model, the section of the pipe is supposed constant and the celerity of waves is independent of the geometric and mechanical properties of the pipe. Furthermore, in this study, the relationship between the pressure and stress has not been developed and the circumferential stress has not been analyzed for different hydrogen mass fraction. During the permanent regime, hydrogen injection will have no effect on the pressure behaviour and on the mechanical strength of the natural gas systems [2, 3]. However, during transient situations, the inner pressure and the stresses along the pipe will have different behaviour. It is important to mention that exceeding the yield strength

will cause the pipe's rupture and hence hydrogen's release to the atmosphere. Hydrogen-air mixtures are extremely easy to ignite requiring only 0.017 mJ ignition energy compared to 0.25 mJ for hydrocarbons [4]. In fact, the possibilities of spontaneous ignition of the released hydrogen and the risks associated are well studied in [5–7]. In order to avoid these dangerous situations, it is important to determine to what extent it is possible to mix hydrogen with natural gas in order to not exceed the yield strength of the existing pipelines normally used to pump natural gas.

The aim of this paper is the study of the transient flow of high pressure hydrogen-natural gas mixtures through pipelines. The relationship between the circumferential stress and the pressure is developed taking into account the fluid-structure interaction. In order to determine to what extent it is possible to mix hydrogen with natural gas, the circumferential stress is compared to the yield strength of two commonly used pipeline steels for natural gas transportation: the X52 and X70 steels.

In this study, the transient regime is created by the rapid closure of a downstream shut-off valve. The governing equations for such flows are two coupled nonlinear hyperbolic partial differential equations. These equations are developed by considering two models: the deformable model which takes into account the elasticity of the pipe and the rigid model considering the pipe to be rigid. The numerical resolution of the governing equations is performed by method of characteristics [3].

2. Assumptions

The mathematical model is based on the following assumptions: the flow is compressible and includes rapid transients, variations in potential energy may be ignored and the viscous effects are modelled by considering friction between the gas and pipeline wall. The calculation of the pressure loss is done by analogy with the permanent flows.

The transient flow is supposed one-dimensional and concerns a homogeneous fluid mixture of hydrogen and natural gas. The hydrogen-fluid mass ratio is noted $\theta = [M_h(M_g + M_h)]$,where M_h and M_g represent the masses of hydrogen and natural gas respectively. The densities of hydrogen and natural gas evolve according to the following adiabatic process:

$$\frac{p}{\rho_h^{\gamma}} = \text{constant}, \tag{2.1}$$

$$\frac{p}{\rho_g^{\gamma'}} = \text{constant}, \tag{2.2}$$

where p is the pressure of the mixture, ρ_h and ρ_g are the hydrogen and the natural

gas densities respectively, γ and γ' are the specific heats ratios for hydrogen and natural gas respectively defined as the ratio of the specific heat at constant pressure C_p and the specific heat at constant volume C_V for each gas.

Equations (2.1) and (2.2) are also valid for the known values of the initial conditions.

$$\frac{p_0}{\rho_{h_0}^{\gamma}} = \text{constant}, \tag{2.3}$$

$$\frac{p_0}{\rho_{g_0}^{\gamma'}} = \text{constant}. \tag{2.4}$$

The subscript 0 refers to the initial conditions.

Equalizing equations (2.1) and (2.3) for hydrogen, equations (2.2) and (2.4) for natural gas, one obtains a relationship describing the pressure and the density evolution as function of the initial conditions:

$$\rho_h = \rho_{h_0}\left(\frac{p}{p_0}\right)^{1/\gamma}, \tag{2.5}$$

$$\rho_g = \rho_{g_0}\left(\frac{p}{p_0}\right)^{1/\gamma'}. \tag{2.6}$$

3. Mathematical formulation

3.1. Equations of motion

By application of mass and momentum conservation laws to an element of fluid between two sections of abscissa x and $x+dx$ of the pipe, the equations describing one-dimensional adiabatic compressible gas can be written as follows [8]:

$$\frac{\partial \rho A}{\partial t} + \frac{\partial \rho A V}{\partial x} = 0, \tag{3.1}$$

$$\frac{\partial \rho V}{\partial t} + \frac{\partial (\rho V^2 + p)}{\partial x} + \frac{\lambda \rho V |V|}{2D} = 0, \tag{3.2}$$

where λ is the coefficient of friction between the gas and pipeline wall, V the velocity of the mixture, ρ the mixture density, p the pressure, D the pipe's diameter and A its cross-sectional area.

3.2. Expression of the mixture density

The expression of the average density of the mixture is defined with respect to the hydrogen mass ratio θ [9]:

$$\rho = \left[\frac{\theta}{\rho_h} + \frac{1-\theta}{\rho_g}\right]^{-1} = \left[\frac{\theta}{\rho_{h_0}}\left(\frac{p_0}{p}\right)^{1/\gamma} + \frac{(1-\theta)}{\rho_{g_0}}\left(\frac{p_0}{p}\right)^{1/\gamma'}\right]^{-1}. \tag{3.3}$$

3.3. Deformable model

Assuming only principal deformations, the three constitutive equations describing the relationship between strains and stresses are

$$\varepsilon_L = \frac{\sigma_L}{E} - \nu\frac{\sigma_\theta + \sigma_R}{E}, \tag{3.4}$$

$$\varepsilon_\theta = \frac{\sigma_\theta}{E} - \nu\frac{\sigma_L + \sigma_R}{E}, \tag{3.5}$$

$$\varepsilon_R = \frac{\sigma_R}{E} - \nu\frac{\sigma_L + \sigma_\theta}{E}, \tag{3.6}$$

where ε_L, ε_θ and ε_R are the longitudinal strain, circumferential strain and radial strain respectively, σ_L, σ_θ and σ_R are the longitudinal stress, circumferential stress and radial stress respectively, ν is the Poisson coefficient and E is the Young's modulus of elasticity.

By considering a plane stress assumption, the radial stresses along the pipe can be neglected. In this case:

$$\sigma_R = 0. \tag{3.7}$$

We assume that there is no elongation of the pipe, in this case we have:

$$\varepsilon_L = 0. \tag{3.8}$$

Taking into account equations (3.7) and (3.8), equations (3.4)–(3.6) become respectively:

$$\sigma_L = \nu\sigma_\theta, \tag{3.9}$$

$$\varepsilon_\theta = \frac{\sigma_\theta}{E} - \nu\frac{\sigma_L}{E}, \tag{3.10}$$

$$\varepsilon_R = -\nu\frac{\sigma_L + \sigma_\theta}{E}. \tag{3.11}$$

By considering that $e/D \ll 1$, the circumferential strain is given by the following equation:

$$\varepsilon_\theta = \frac{D - D_0}{D_0}. \tag{3.12}$$

The radial strain is given by the following equation:

$$\varepsilon_R = \frac{e - e_0}{e_0}. \tag{3.13}$$

In the two above equations, e and D are the thickness and diameter of the deformed pipe respectively, e_0 and D_0 are the initial thickness and diameter of the pipe respectively.

By assuming that stress variations along the pipe are sufficiently small to be neglected in deriving formulas for stresses, in particular, the circumferential stress is given by Laplace's law as follows:

$$\sigma_\theta = \frac{pD}{2e}. \tag{3.14}$$

Taking into account (3.12), the combination of (3.9) and (3.10) leads to

$$\frac{D - D_0}{D_0} = (1 - \nu^2)\frac{\sigma_\theta}{E}. \tag{3.15}$$

Taking into account (3.13), the combination of (3.9) and (3.11) leads to

$$\frac{e - e_0}{e_0} = -\nu(1 + \nu)\frac{\sigma_\theta}{E}. \tag{3.16}$$

By combining Eqs. (3.15) and (3.16) to eliminate σ_θ/E, the following equation is obtained:

$$\frac{D - D_0}{D_0} = \frac{\nu - 1}{\nu}\,\frac{e - e_0}{e_0}. \tag{3.17}$$

By introducing (3.14) and (3.17) in (3.15), we obtain

$$\psi D^2 + \left(e_0 - 2\psi D_0 - \frac{D_0(1 - \nu^2)}{2E}p\right)D + \psi D_0^2 - e_0 D_0 = 0, \tag{3.18}$$

where $\psi = \nu e_0/(D_0(\nu - 1))$.

Equation (3.18) describes the relationship between the pressure and the diameter of the pipe.

Expression of the celerity of pressure waves in deformable pipes. The celerity of the pressure waves in the fluid can be defined by the expression [10]:

$$C = \left(\frac{\partial \rho}{\partial p} + \frac{\rho}{A}\frac{\partial A}{\partial p}\right)^{-1/2}, \tag{3.19}$$

where $A = \pi D^2/4$ is the cross-sectional area of the pipe.

The first term of the right side of equation (3.19) can be obtained by differentiation of equation (3.3):

$$\begin{aligned}\frac{\partial \rho}{\partial p} = &\left[\frac{\theta}{\rho_{h_0}}\left(\frac{p_0}{p}\right)^{1/\gamma} + \frac{(1 - \theta)}{\rho_{g_0}}\left(\frac{p_0}{p}\right)^{1/\gamma'}\right]^{-2} \\ &\times \frac{1}{p}\left[\frac{1}{\gamma}\frac{\theta}{\rho_{h_0}}\left(\frac{p_0}{p}\right)^{1/\gamma} + \frac{1}{\gamma'}\frac{(1 - \theta)}{\rho_{g_0}}\left(\frac{p_0}{p}\right)^{1/\gamma'}\right].\end{aligned} \tag{3.20}$$

The second term of the right side of (3.19) is obtained by differentiation of equation (3.18). The following equation can be obtained:

$$\frac{1}{A}\frac{\partial A}{\partial p} = \frac{D_0(1-\nu^2)/2E}{\psi(D-D_0)+e_0/2-pD_0(1-\nu^2)/4E}. \tag{3.21}$$

By substituting equations (3.20), (3.21) and (3.3) in equation (3.19), the celerity of waves can be obtained as a function of the pressure.

3.4. Rigid model

In this case, the cross-section A of the pipe is considered constant:

$$A = \frac{\pi D^2}{4} = \frac{\pi D_0^2}{4} = cte. \tag{3.22}$$

The celerity of waves is simplified [3]:

$$C = \left(\frac{\partial \rho}{\partial p}\right)^{-1/2} = \left[\frac{\theta}{\rho_{h_0}}\left(\frac{p_0}{p}\right)^{1/\gamma} + \frac{(1-\theta)}{\rho_{g_0}}\left(\frac{p_0}{p}\right)^{1/\gamma'}\right] \times \left[\frac{1}{p}\left[\frac{1}{\gamma}\frac{\theta}{\rho_{h_0}}\left(\frac{p_0}{p}\right)^{1/\gamma} + \frac{1}{\gamma'}\frac{(1-\theta)}{\rho_{g_0}}\left(\frac{p_0}{p}\right)^{1/\gamma'}\right]\right]^{-1/2}. \tag{3.23}$$

4. Numerical solution by the method of characteristics

The method of characteristics [11] is applied to the PDEs (3.1) and (3.2), and the partial differential terms associated with the flow velocity and the pressure are then reduced to ordinary differential ones compatible with two characteristic lines C^+ and C^- (Fig. 1). The ordinary differential equations of (3.1) and (3.2) are

$$C^+ \begin{cases} dV + \dfrac{1}{\rho C}dp = -Jdt, \\ \dfrac{dx}{dt} = (V + C), \end{cases} \tag{4.1}$$

$$C^- \begin{cases} dV - \dfrac{1}{\rho C}dp = -Jdt, \\ \dfrac{dx}{dt} = (V - C), \end{cases} \tag{4.2}$$

where $J = \lambda V|V|/2D$ represents the pressure loss by unit of pipe length. In this term, the diameter D is a function of the pressure determined by solving the quadratic equation (3.18).

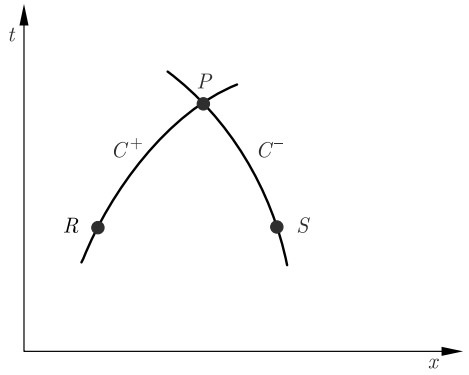

FIG. 1. Characteristics lines.

Equations (4.1) and (4.2) determine the evolution of the pressure and the velocity according to the time and the space. One solves these equations by using first-order finite-difference approximations. Consider conditions known (V, p, x, t) at points R and S (Fig. 1). The two characteristics C^+ and C^- passing through R and S, intersect at point P where conditions are unknown. Using the linear finite-difference form between points P and R for equations (4.1) and between P and S for equations (4.2), one obtains the following equations:

$$V_P - V_R + \left(\frac{1}{\rho C}\right)_R (p_P - p_R) + J_R(t_P - t_R) = 0, \tag{4.3}$$

$$x_P - x_R = (V + C)_R(t_P - t_R), \tag{4.4}$$

$$V_P - V_S - \left(\frac{1}{\rho C}\right)_S (p_P - p_S) + J_R(t_P - t_S) = 0, \tag{4.5}$$

$$x_P - x_S = (V - C)_S(t_P - t_S). \tag{4.6}$$

The subscripts are used to define the location of the known or the unknown quantity. These four equations suffice, a priori, to find the unknown t_P, x_P, V_P and p_P, and hence to determine a solution if the points R and S are judiciously selected so that the difference equations adequately represent the original differential equations. However, the C^+ and C^- characteristic lines appear as curved lines on the x-t plane (Fig. 1) in view of the fact that the celerity of waves C is a function of the pressure p. Thus, an iterative trapezoidal rule is applied to ameliorate the solution of the first approximation given by equations (4.3)–(4.6). Consequently, we obtain the unknown values t_P, x_P, V_P and p_P at the point P:

$$t_P^k = \frac{x_S - x_R + F_R t_R - G_S t_S}{F_R - G_S}, \tag{4.7}$$

$$x_P^k = x_R + F_R(t_P^k - t_R), \tag{4.8}$$

$$p_P^k = \frac{[M_R p_R + M_S p_S + V_R - V_S + H_R(t_P^k - t_R) - H_S(t_P^k - t_S)]}{M_R + M_S}, \tag{4.9}$$

$$V_P^k = V_R + M_R(p_R - p_P^k) + H_R(t_P^k - t_R), \tag{4.10}$$

where: $F_R = (V + C)_R$, $G_S = (V - C)_S$, $M_{R,S} = (1/\rho C)_{R,S}$, $H_{R,S} = -J_{R,S}$ for $k = 1$ and $F_R = 1/2[(V+C)_P^{k-1} + (V+C)_R]$, $G_S = 1/2[(V-C)_P^{k-1} + (V-C)_S]$, $M_{R,S} = 1/2[(1/\rho C)_P^{k-1} + (1/\rho C)_{R,S}]$, $H_{R,S} = 1/2[(-J)_P^{k-1} + (-J)_{R,S}]$ for $k = 2, \ldots, j$.

In this study, the iteration number is limited to $j = 20$. The determination of the solution in the two extreme sections imposes the introduction of the appropriate boundary conditions.

5. Application and results

5.1. Description of the system and formulation of the problem

To illustrate the dynamic behavior of high-pressure hydrogen-natural gas mixtures in pipelines, an installation composed of a compressor pumping the mixture through a single steel pipeline 500 m long and a Young's modulus $E = 2 \times 10^{11}$ Pa is considered (Fig. 2). To analyze the effect of the geometric properties on the pressure and the circumferential stress evolution, two different diameters of the pipe are considered (Table 1).

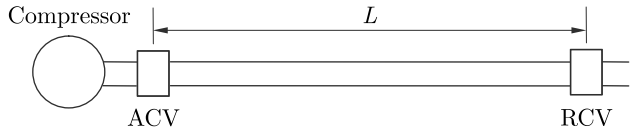

FIG. 2. Hydrogen-natural gas mixtures installation.

Table 1. Geometric properties of the pipe.

	Outer diameter	Wall thickness 'e'
1	600 mm	11 mm
2	400 mm	6 mm

In the event of a sudden emergency, we close the rapid closure valve (RCV) at the downstream end. In this case, the pressure in the supply line may reach excessive values and may destroy the compressor and the pipeline. To avoid this, an automatic closure valve (ACV) is placed at the immediate discharge side of the compressor. As initial condition, a mass flow is assumed equal to $m_0 = 20$ Kg/s, a static temperature $T = 15°$C and an absolute pressure $p = 70$ bar.

The properties of hydrogen and natural gas used in the calculations are presented in Tables 2 and 3 respectively.

Two parameters are used to characterize the dynamic response of the valves: the reaction time (time taken to start the valve actuation after sensing a pressure perturbation) and the actuation time (time interval between the initial and the final positions of the valve). For the RCV valve we considered the actuation time only. Table 4 summarizes these closure times.

Table 2. Hydrogen properties in working conditions, $p = 70$ bar and $T = 15°$C.

Symbol	Designation	Value	Unit
C_p	specific heat at constant pressure	14600	J/(Kg · °K)
C_v	specific heat at constant volume	10440	J/(Kg · °K)
R	gas constant	4160	J/(Kg · °K)

Table 3. Natural gas properties in working conditions, $p = 70$ bar and $T = 15°$C.

Symbol	Designation	Value	Unit
C_p	specific heat at constant pressure	1497.5	J/(Kg · °K)
C_v	specific heat at constant volume	1056.8	J/(Kg · °K)
R	gas constant	440.7	J/(Kg · °K)

Table 4. Reaction and actuation time of valves.

Case	ACV reaction	ACV actuation	RCV actuation
1	0.2 s	0.5 s	0.2 s
2	2 s	5 s	0.2 s
3	4 s	10 s	0.2 s

Figures 3 and 4 show plots of the numerically obtained results for the mass-flow, as function of time, for two sections at the exit side of the (ACV) and immediately at the upstream end of the RCV, for cases 1, 2 and 3 and for the pipe of diameter 0.4 m. After the rapid closure of the RCV, a pressure wave front propagates towards the upstream end of the pipeline and makes the ACV react and start to close [3]. Since the celerity of waves is proportional to the mass fraction θ, it takes less time to reach the ACV valve when θ increases. In fact, the interval τ, which equals the sum of the reaction time, the actuation time and the time that takes the waves to reach the ACV, is greater in the case of natural gas ($\theta = 0$) than that in the case of hydrogen ($\theta = 1$) as shown in Fig 3.

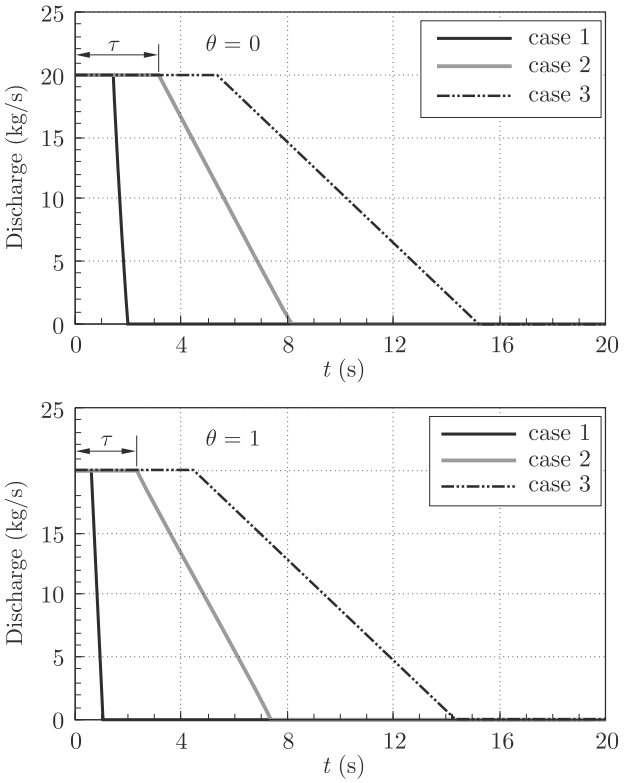

FIG. 3. Mass flow rate as a function of time at the ACV side, for cases 1, 2 and 3 for $\theta = 0$ and for $\theta = 1$ and for $D = 0.4$ m.

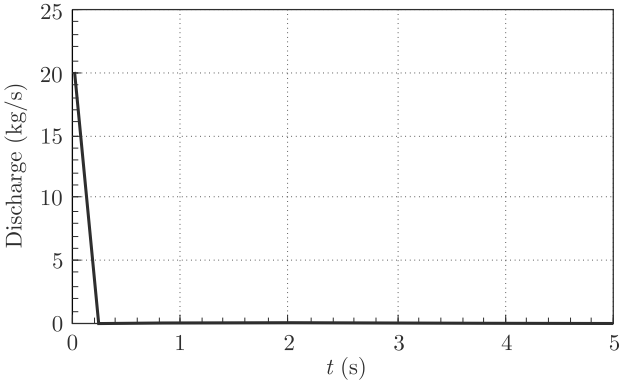

FIG. 4. Mass flow rate as a function of time at the RCV side and for $D = 0.4$ m.

5.2. Comparison between the rigid and the deformable models

To compare the rigid and the deformable models, referring to the installation of Fig. 2, the transient flow of hydrogen-natural gas mixtures is analyzed for

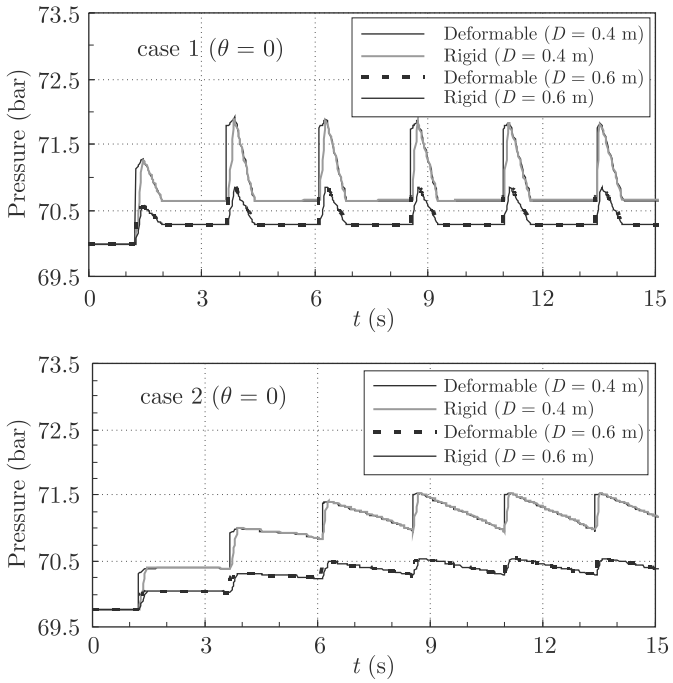

Fig. 5. Pressure as a function of time, for cases 1 and 2 at the ACV side, for $\theta = 0$.

a steel pipeline with two different diameters as shown in Table 1. Figures 5 and 6 show plots of the numerically obtained results for the pressure distribution at the ACV side, as a function of time, for the cases 1, 2 and 3 of the valves closure time, and for $\theta = 0$ and $\theta = 1$. These figures show a good agreement between the rigid model and the deformable model for the different values of θ, for the three cases of the valves closure and for the two diameters of the pipeline. Figures 5 and 6 also show that the pressure is proportional to θ and to the valves closure time and inversely proportional to D. It is important to mention that during the valves closure, two pressure waves of opposite signs are created. A compression wave at the down-stream end valve (RCV) and a depression wave at the upstream end valve (ACV). These waves propagate along the pipe with the same speed and they are reflected at both ends of the pipe without changing their signs. When the time evolves, due to the friction, the phenomenon of wave propagation and reflection will be damped. During their passage at the different sections of the pipe, the compressive wave causes the pressure increase and the depression wave causes the pressure decrease. In fact, the serrations observed in the plots of Figs. 5 and 6 well explain the increase and the decrease of the pressure caused by these waves.

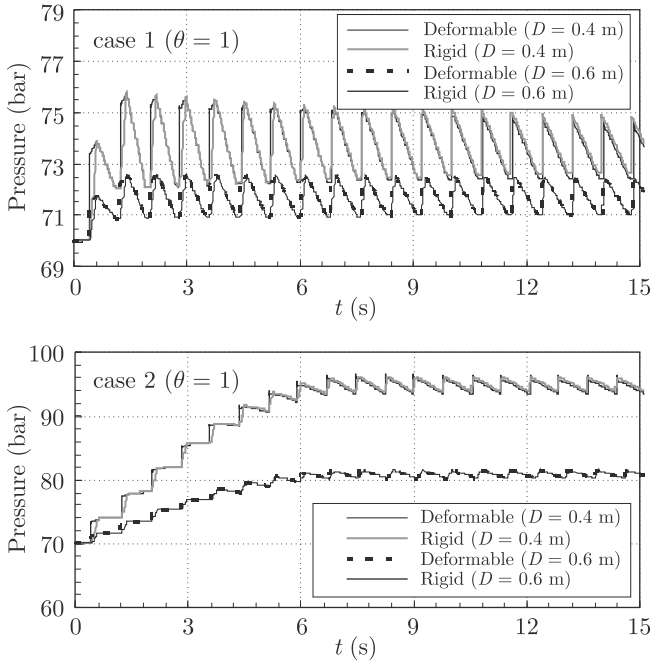

FIG. 6. Pressure as a function of time, for cases 1 and 2 at the ACV side, for $\theta = 1$.

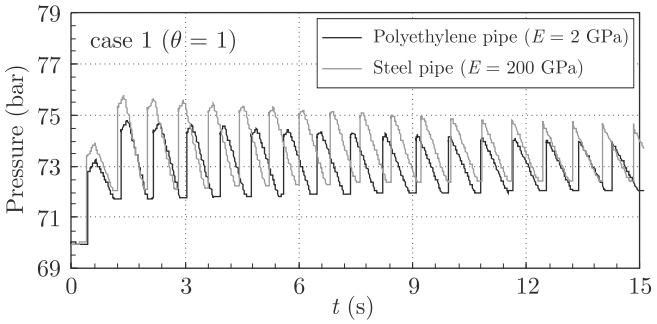

FIG. 7. Comparison of the pressure evolution between a polyethylene pipe and a steel pipe, at the ACV side, for the case 1 and for $\theta = 1$.

From these figures, the good agreement between the two numerical models allows to state that the elasticity of the pipes has a negligible effect in the case of steel pipelines. However, in the case of elastic pipes such as pipes made of polyethylene, the deformability of the pipe wall can not be neglected. In fact, Fig. 7 shows a comparison of the pressure evolution between a steel pipe and a polyethylene pipe ($E = 2 \times 10^9$ Pa) which have the same geometric properties ($D = 0.4$ m, $e = 6$ mm), for the case 1, at the ACV side and for $\theta = 1$.

The obtained results clearly show the effect of the elasticity on the pressure. It can be noted that the maximum pressure is 75.8 bar for the steel pipe, while it is reduced in the case of the polyethylene pipe to reach the value of 74.5 bar. Hence, the deformable model is general since it takes into account the compressibility of the fluid and the deformability of the pipe's wall. In the following, the deformable model is adopted.

5.3. Effect of hydrogen mass fraction on the circumferential stress

To introduce the mechanical properties of the pipe, two API grade pipeline steels X52 and X70 are considered (Table 5). The steel X52 is the most frequently used in existing gas pipelines and the X70 steel is the object of implementation into new pipeline systems [2]. The mechanical properties σ_u, σ_y and σ, defined in Table 5, are the ultimate strength, the yield strength and the allowable strength respectively. The allowable strength is determined by considering a safety factor equals to 2 as mentioned in Table 5.

Table 5. Mechanical properties of steels in air.

Steel grade	σ_u, MPa	σ_y, MPa	$\sigma = \sigma_y/2$, MPa
X52	528	410	205
X70	712	590	295

Figures 8 and 9 show plots of the numerically obtained results for the circumferential stress evolution as a function of time at the ACV side, for the cases 1, 2 and 3 of the valves closure, for different values of hydrogen mass ratio θ, and for different diameters of the pipe. These plots show the influence of the hydrogen mass fraction θ on the circumferential stress evolution. In fact, it can be noted on Fig. 8 and for the case 1, the maximum stress in the case of natural gas ($\theta = 0$) is 193.6 MPa. In the case of hydrogen-natural gas mixtures, the maximum stress is 195.4 MPa for $\theta = 1/3$ and 197 MPa for $\theta = 2/3$. For hydrogen ($\theta = 1$), the maximum stress is 198 MPa. The results of the numerical simulation plotted in Figs. 8 and 9 show that the circumferential stress is inversely proportional to the diameter of the pipe.

Figure 8 shows that for the different cases of the valves closure time and for the different values of θ, the circumferential stress evolution has not exceeded the allowable stress of X70 steel ($\sigma = 295$ MPa). Figure 8 shows also that for the case 1 and for the different values of θ, the circumferential stress evolution has not exceeded the allowable stress of X52 steel ($\sigma = 205$ MPa). However, in the second case of the valves closure time, and in order to not exceed the allowable stress of the X52 steel, the maximum hydrogen mass fraction permitted in the

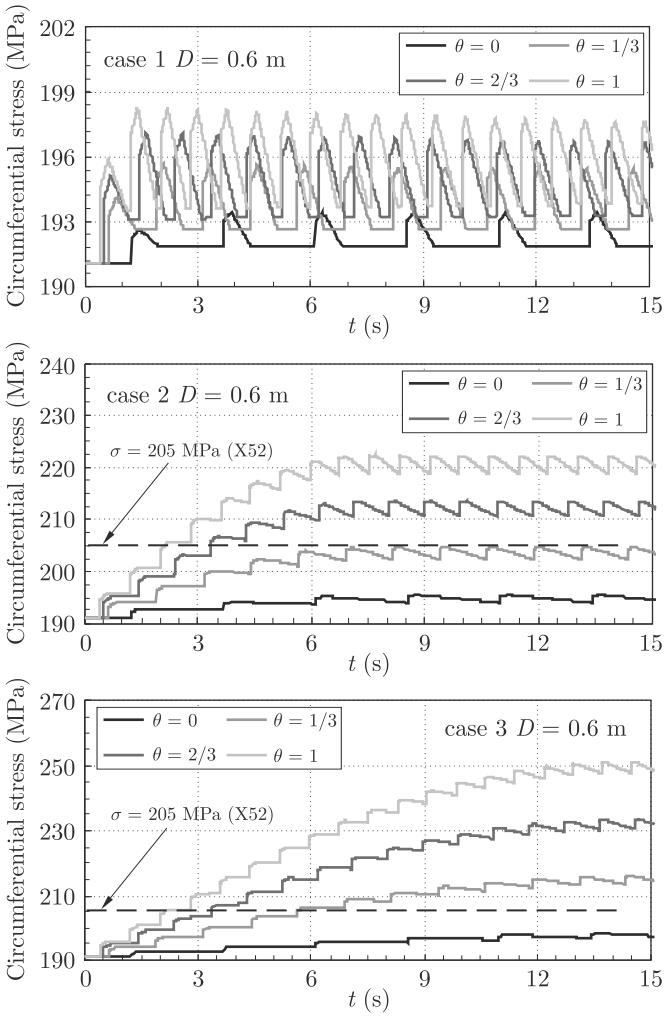

FIG. 8. Circumferential stress as a function of time, for cases 1, 2 and 3 at the ACV side, for $D = 0.6$ m and for different values of θ.

mixture is about the third. While for the case 3, the allowable stress of the X52 steel has been exceeded in all cases of hydrogen-natural gas mixtures as shown in Fig. 8.

Figure 9 shows that the circumferential stress has exceeded the allowable stress of the X52 steel ($\sigma = 205$ MPa) for the different hydrogen mass fractions θ and for the three cases of the valves closure. This figure shows also that for the first case of the valves closure and for the different values of θ, the circumferential stress evolution has not exceeded the allowable stress of the X70 steel ($\sigma = 295$ MPa). However, in the second case of the valves closure, and in

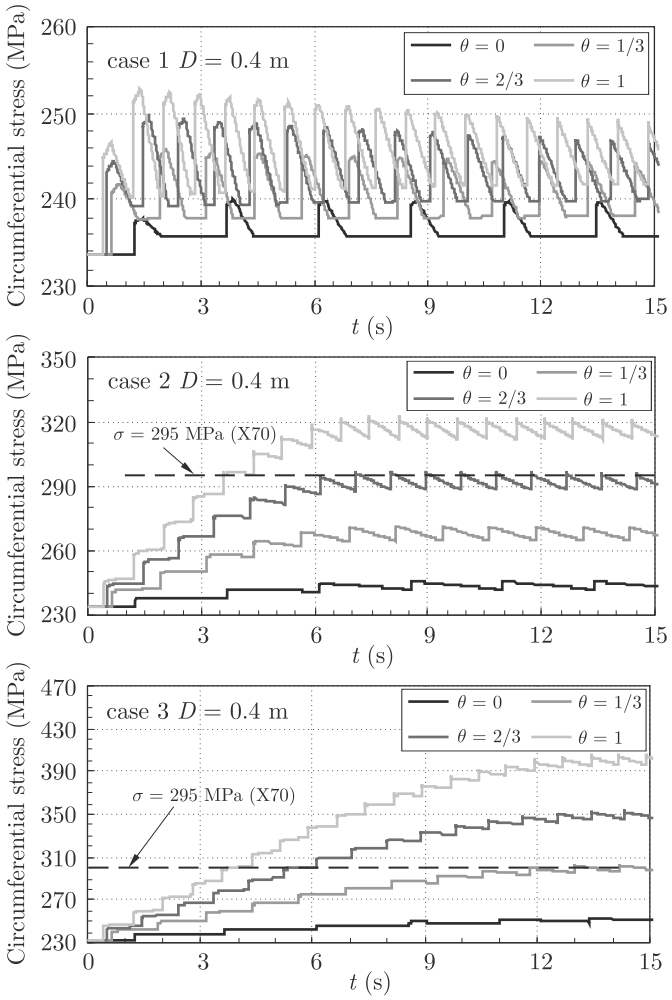

Fig. 9. Circumferential stress as a function of time, for cases 1, 2 and 3 at the ACV side, for $D = 0.4$ m and for different values of θ.

order to not exceed the allowable stress of the X70 steel, the maximum hydrogen mass fraction θ permitted in the mixture is $2/3$ and it is reduced to the third in the case 3 as shown in Fig. 9.

The numerically obtained results confirm that even if the internal stress has not exceeded the allowable stress of the pipe during the permanent regime, further studies should be performed during transient situations and for different percentages of hydrogen mass fraction and by considering different safety factors. The safety factor should be correctly chosen by taking into account the changes of the mechanical properties of the pipe that could occur due to the presence of hydrogen and by respecting the different codes.

6. Conclusions

In this study, the numerical solution of the transient flow in natural gas pipelines of hydrogen-natural gas mixtures has been presented. This problem is governed by two coupled nonlinear partial differential equations of hyperbolic type. The numerical method employed is the method of characteristics. The boundary conditions were imposed by introducing a linear closure law for the upstream and the downstream valves. The occurrence of pressure oscillations in the upstream side of the pipe was analyzed as a result of the compression wave originated by the rapid closure of downstream valve (RCV). In this case, the pressure may reach excessive values due to the mass accumulation effect caused by the delay of the upstream valve closure. The effect of the different values of hydrogen mass fraction on the dynamic behaviour of the pressure and the circumferential stress were also analyzed. The obtained results show that the transient pressure for hydrogen and hydrogen-natural gas mixtures are higher compared to natural gas. Additionally, these results show that the allowable stress of the natural gas pipelines is exceeded for some fractions of hydrogen in the hydrogen-natural gas mixtures. Therefore, attention should be paid when mixing hydrogen with natural gas in the existing pipelines designed for natural gas only.

References

1. C. SAN MARCHI, B.P. SOMERDAY, S.L. ROBINSON, *Permeability, solubility and diffusivity of hydrogen isotopes in stainless steel at high pressures*, International Journal of Hydrogen Energy, **2**, 100–116, 2006.

2. J. CAPELLE, I. DMYTRAKH, G. PLUVINAGE, *Comparative assessment of electrochemical hydrogen absorption by pipeline steels with different strength*, Corrosion Science, **2**, 1554–1559, 2010.

3. S. ELAOUD, E. HADJ TAÏEB, *Transient flow in pipelines of high-pressure of hydrogen-natural gas mixtures*, International Journal of Hydrogen Energy, **33**, 4824–4832, 2008.

4. AIGA Document, *Hydrogen transportation pipelines*, Asia Industrial Gases Association, 2006, Available from: http://www.asiaiga.org.

5. J. B. SAFFERS, V.V. MOLKOV, *Towards hydrogen safety engineering for reacting and non-reacting hydrogen releases*, Journal of Loss Prevention in the Process Industries, 7–11, 2011 (to appear).

6. P. XU, J. ZHENG, P. LIU, R. CHEN, F. KAI, L. LI, *Risk identification and control of stationary high-pressure hydrogen storage vessels*, Journal of Loss Prevention in the Process Industries, **22**, 950–953, 2009.

7. B.P. XU, J.X. WHEN, S. DEMBELE, V.H.Y. TAMB, S.J. HAWKSWORTH, *The effect of pressure boundary rupture rate on spontaneous ignition of pressurized hydrogen release*, Journal of Loss Prevention in the Process Industries, **22**, 279–287, 2009.

8. E.B. Wylie, V.L. Streeter, L.Suo, *Fluid Transients in Systems*, Prentice Hall, Englewood Cliffs, NJ, 1993.

9. E. Hadj-Taïeb, T. Lili, *The numerical solution of the transient two-phase flow in rigid pipelines*, International Journal For Numerical Methods in Fluids, **29**, 501–514, 1999.

10. S. Stuckenbruck, D.C. Wiggert, R.S. Otwell, *The influence of pipe motion on pressure wave propagation*, ASME Journal of Fluids Engineering, **7**, 518–522, 1985.

11. M.B. Abbott, *An Introduction to the Method of Characteristics*, American Elsevier, New York, 1966.

Received November 5, 2013; revised version March 5, 2014.